ICSE6-042

Edge scour in current adjacent to stone covers

Thor Ugelvig PETERSEN[1], B. Mutlu SUMER[2], Knud Erik MEYER[3], Jørgen FREDSØE[4] and Erik D. CHRISTENSEN[5]

[1]PhD-student. Technical University of Denmark, DTU Mekanik, Section for Fluid Mechanics, Coastal and Maritime Engineering. DK-2800 Kgs. Lyngby: tupe@mek.dtu.dk

[2]Professor. Technical University of Denmark, DTU Mekanik, Section for Fluid Mechanics, Coastal and Maritime Engineering. DK-2800 Kgs. Lyngby: bms@mek.dtu.dk

[3]Associate Professor. Technical University of Denmark, DTU Mekanik, Section for Fluid Mechanics, Coastal and Maritime Engineering. DK-2800 Kgs. Lyngby: kem@mek.dtu.dk

[4]Professor. Technical University of Denmark, DTU Mekanik, Section for Fluid Mechanics, Coastal and Maritime Engineering. DK-2800 Kgs. Lyngby: jf@mek.dtu.dk

[5]Professor. Technical University of Denmark, DTU Mekanik Section for Fluid Mechanics, Coastal and Maritime Engineering. DK-2800 Kgs. Lyngby: edch@mek.dtu.dk

ABSTRACT

The present paper reports some early results of an experimental investigation of edge scour in currents. Two kinds of measurements are made (1) Particle Image Velocimetry (PIV) measurements of secondary currents that take place near a junction between the stone cover and the sand bed in a clear-water experiment; and (2) scour measurements in actual scour experiment in the live-bed regime.

The early results indicate that edge scour in a steady current propagating in-line with a stone layer is caused by the combined action of two effects; (1) Primary flow and (2) Secondary flow. The primary flow stirs up the sediment and puts into suspension, and the secondary flow carries it away from the junction between the stone layer and the sand bed, resulting in a scour hole forming adjacent to the toe of the stone layer.

Key words

Edge scour, cover stones, steady current, scour protection, coastal structures, offshore structures, scour, offshore wind farm.

I INTRODUCTION

Scroby Sands wind farm located in the North Sea 2.5 km off the coast of Great Yarmouth, UK, utilized a scour protection system with rock dump around the monopiles. Surveys made in 2004-2005 show a strong deformation of the scour protection layer comprising both sinking of the stone layer and considerable edge scour (Whitehouse et al., 2011). The design principles of the scour protection implemented in the Scroby Sands wind farm have been described in Hansen and Gislason (2005).

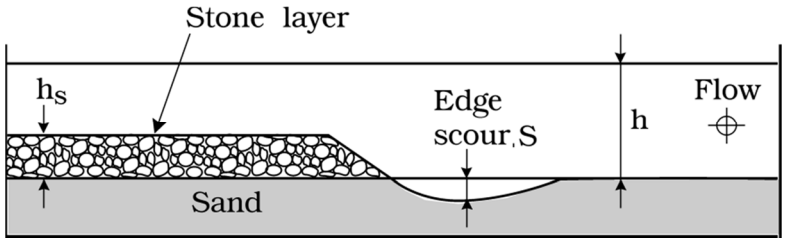

Figure 1: Definition sketch

Figure 1 illustrates the edge scour adjacent to a stone layer placed on a sandy bottom. As pointed out by several investigators, e.g. Fredsøe et al. (2001) and Raaijmakers et al. (2010), edge scour is in fact expected from the design considerations, but so far the mechanisms causing edge scour have not been fully established.

To address this issue an extensive program of physical model tests is in progress. The purpose of the study is to gain an understanding of the stability of stone covers and the scour adjacent to the side edges. This paper presents some early results obtained in the aforementioned experimental campaign.

II EXPERIMENTAL SETUP

The experiments were carried out in a current flume. The flume was 2.0 m wide, 0.5 m deep and 28 m long. The water depth was h = 30 cm. The current was achieved by recirculating water in the flume.

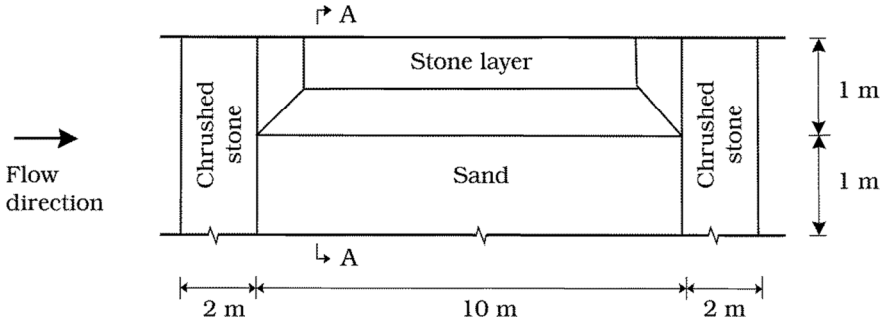

Figure 2: Experimental setup, Plan view

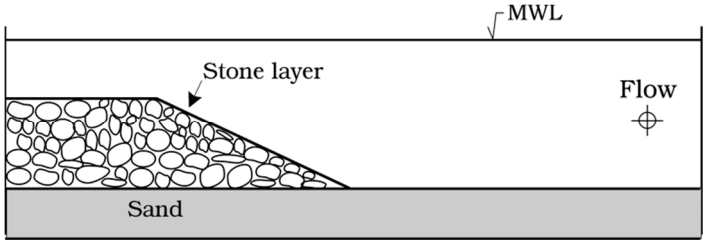

Figure 3: Cross-sectional view, A-A in Figure 2.

A sediment section in the form of a sand pit with two ramps at the two ends was formed in the flume. The sand pit was 2 m wide, 0.15 m deep and 10 m long (see Figure 2), the distance from the upstream end of the sand pit to the inlet section being 7.5 m. The two end ramps (with 1:15 slope) were made from round stones the size 4 cm. The grain size of the sediment (fine sand) used in the experiments was d_{50} = 0.17 mm with a geometric standard deviation of $\sigma_g = d_{84}/d_{50}$ = 1.3.

A stone layer was placed on top of the sand covering half of the flume width in the cross-sectional direction extending over the entire longitudinal direction of the sand pit. At the intersection of the stone layer with the sand a slope α of 1:3 was applied (Figure 3).This slope was adopted to match the stone layer design encountered in practice.

The stone layer was made of crushed angular stones with size D_s = 2.1 cm with a geometric standard deviation of σ_g= 1.2. The experiments were conducted with a stone layer thickness h_s = 18 cm corresponding to N ~ 9 layers of stones.

A mini underwater video camera videotaped the overall time development of the scour process at the toe of stone layer. The movement of the sand grains in the video recordings acted as flow tracers, visualizing the flow structures alongside the toe of the stone layer and the individual stones.

The experiments were run for sufficiently long period of time for the scour process to reach its equilibrium stage. Subsequently, the scour profiles in the cross-flow direction were measured by a laser rangefinder (leicaDisto™ D3a) with a precision of 1 mm and this operation was performed at 10 sections (about 10 cm apart) along the length of the working section.

Velocity measurements by LDA

The velocity profile across the water depth over the sand section was measured, using a Laser Doppler Anemometer (LDA), a Dantec 2D LDA system (Dantec Dynamics, Denmark) comprising a 14 mm "pen-size" submersible probe, the measurements being conducted in backward-scatter mode.

The measurement point was located 7 m away from the beginning of the sand pool and at 0.5 m distance from the side wall. The system was equipped with a BSA F60 Flow Processor and the data was logged in BSA Flow Software v4.50. The data was logged in burst mode which meant the sampling frequency ranged

between 90 – 300 Hz.

The steady current velocity was constantly monitored during the course of the experiment, and the data collected was used to determine the velocity to calculate the quantities such as the depth averaged velocity and the bed friction velocity.

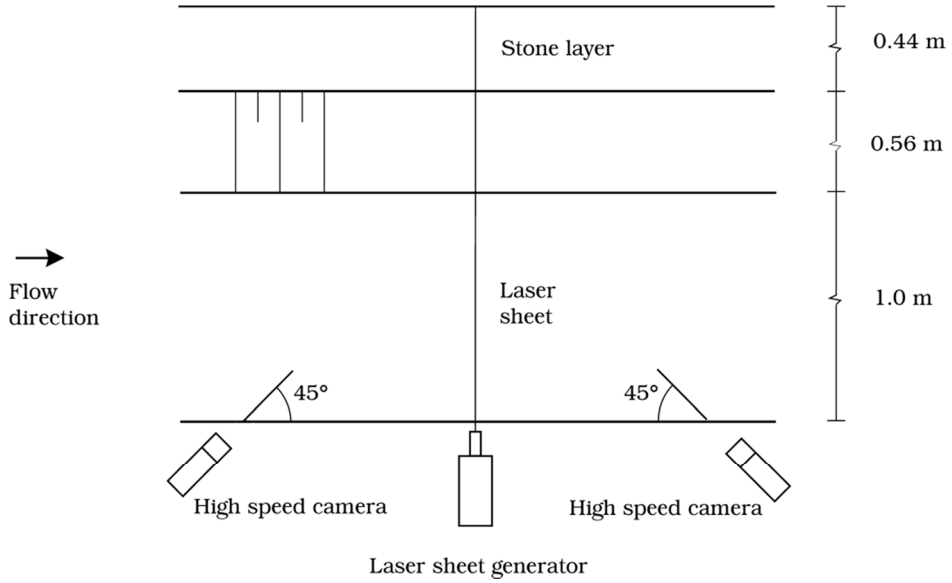

Figure 4: Stereoscopic PIV setup plan view

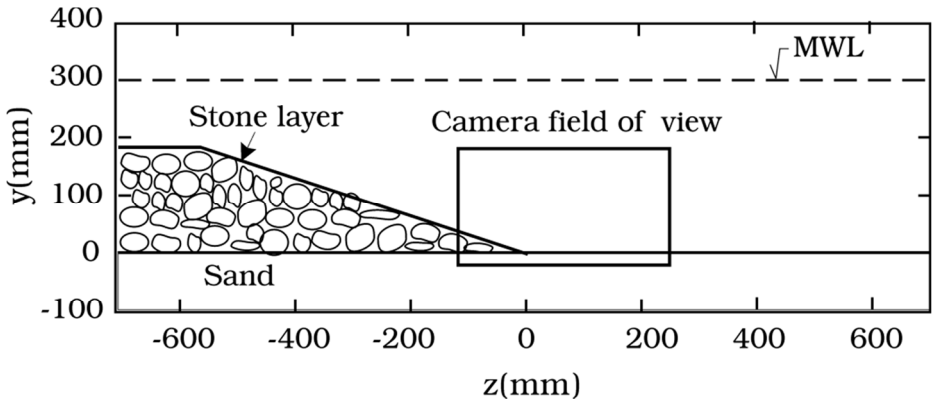

Figure 5: Camera fields of view

Velocity measurements by PIV

Particle Image Velocimetry (PIV) measurements were made to investigate the three-dimensional flow in cross-sectional plane at the junction between the sand and the stone layer. The objectives of the PIV study were twofold: to obtain the secondary currents, and to estimate the turbulence intensity field over the sand and the stone layer. The latter will not be reported in the present paper for reasons of space.

The measurements were made with a PIV system from Dantec Dynamics; the system consisted of two four megapixel cameras, double pulsed (1200 mJ/pulse) Nd:Yag laser, a synchronizer to facilitate system timing and frame grabbers to facilitate image acquisition. The PIV data logging was made in Dynamic Studio v2.50. As shown in Figure 4 the two cameras were mounted alongside the flume side wall viewing the measurement volume at a 45° angle. On the glass side wall for each camera a water prism with an orientation of 45° was mounted in order to eliminate refraction. The laser light sheet was also introduced from the flume side wall aimed directly at the measurement volume.

The PIV measurements were made in the clear-water regime, where no sediment transport occurred (not even adjacent to the stone cover). This ensured that the sediment bed would not change during the execution time, and that larger sediment particles suspended from the bed would not disturb the data collection. This

further allowed acquisition of large ensembles of data. Note that the scour experiment (Test 1 in Table 1) was performed in the live-bed regime.

Given the appreciable amount of data storage and post-processing requirements of the PIV measurements, it was decided to focus on a single stone layer thickness and a specific depth-averaged-velocity flow scheme. The setup was prepared with a flat sediment bed and the experiment was carried out in the clear water regime, and no change in the bed morphology was observed.

For the given setup one camera field of view was measured, so that the flow in the vicinity of the stone layer toe was covered, as illustrated in Figure 5. The calibration images for the field of view were used to provide the dimensional position for the field of view in laboratory coordinates.

At the frame position an ensemble of 5400 image pairs were obtained. The image pairs were subsequently analyzed and interrogated using the Dynamic Studio v2.30. Images were interrogated with 32 x 32 windows, using a 50 % overlap. Typical vector removal rates ranged from 2 to 4 % with the bulk of removed vectors near the sediment bed and the stone layer. In both cases the moderate scattering of laser light from the sediment grains and the stones were responsible. This effect was inevitable despite the effort to minimize it with flat black paint.

III TEST CONDITIONS

Table 1 summarizes the test conditions for the scour tests. In the table the quantity V is the depth averaged current velocity. Note that for test no. 2 the velocity measurements were made within the camera field of view (Figure 5) extending up to h ~ 16 cm above the bed.

The quantity U_f denotes the bed friction velocity determined in the following two ways: (1) from the familiar log-fit exercise using the measured velocity profiles from the PIV measurements; (2) from the flow resistance relation

$$U_f = \sqrt{f/2}\,V \qquad (1)$$

in which f is calculated from the Colebrook-White formula (e.g. Schlichting, 1979) and V was obtained from the LDA measurements described in the previous section. The Shields parameter θ in the table is defined by

$$\theta = \frac{U_f^2}{g(s-1)d_{50}} \qquad (2)$$

n which g is the gravitational acceleration, s the specific gravity of the sediment grains (=2.65).

In the table the quantity S is the scour depth corresponding to the equilibrium stage of the scour process (Figure 1).

Note that the Shields parameter in Test 1 was larger than the critical value corresponding to initiation of motion at the bed, meaning that the scour experiments were conducted in the live-bed regime. This was also revealed by the appearance of ripples on the sediment bed. The Shields parameter in Test 2 was lower than the critical value and no motion on the bed was observed.

Test	Stone size	Number of Stone Layers	Stone layer thickness	Depth Averaged Current Velocity	Friction velocity in steady current	Grain Reynolds number	Shields Parameter	Equilibrium scour depth
	D_s	N	h_s	V	U_f	$d_{50}U_f/\nu$	θ	S
	[cm]	[-]	[cm]	[cm/s]	[cm/s]		[-]	[mm]
1	2.1	9	18	30.5	1.4	2.4	0.072	10
2	2.1	9	18	10.6	0.45	0.76	0.007	-

Table 1: Test conditions

IV RESULTS AND DISCUSSION

Secondary flow

Figure 6 shows the secondary flow structures within the full camera field of view and Figure 7 shows a close-up of the corner section. Previous studies show that secondary flow structures of channel flows can be caused by a sudden change in roughness and corner-induced effects. The sudden change in roughness forces

a secondary current directed from the rough section into the smooth section due to mean flow deflection (Müller and Studerus, 1979). The corner induced secondary current is turbulence-driven (van Rijn, 2011 and Nezu and Nakagawa, 1993), where the flow goes from the main body of the flow towards the corner. The secondary flow very close to the bed in the sand section is directed away from the stone layer toe, and that over the stones are directed into the stone layer. The separation of the flow over the stones highly disturbs the measurements in the local field.

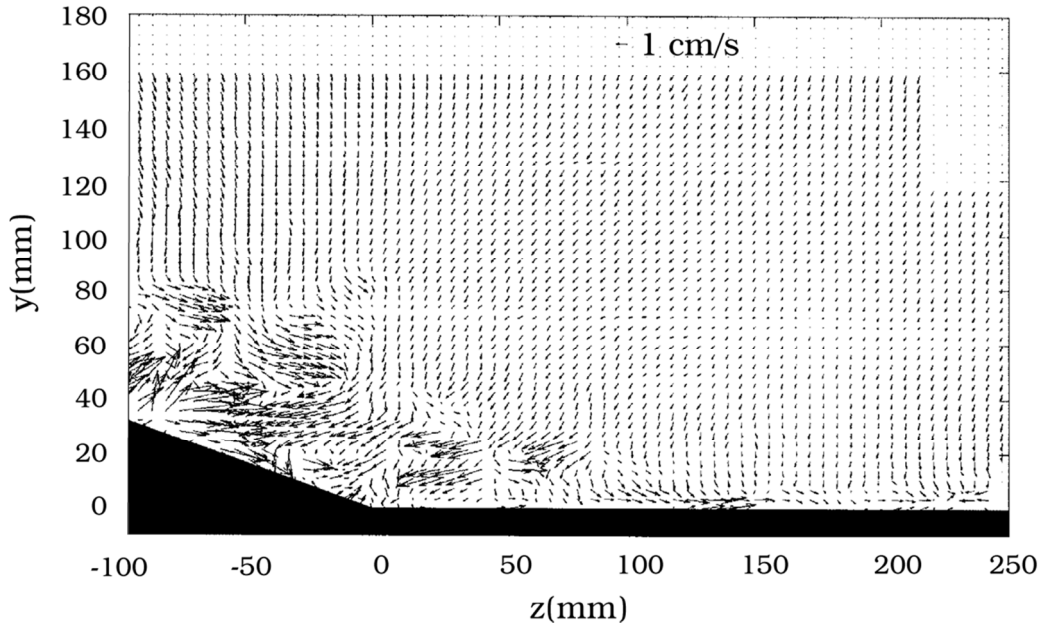

Figure 6: Secondary flow structures in camera field of view. Test 1.

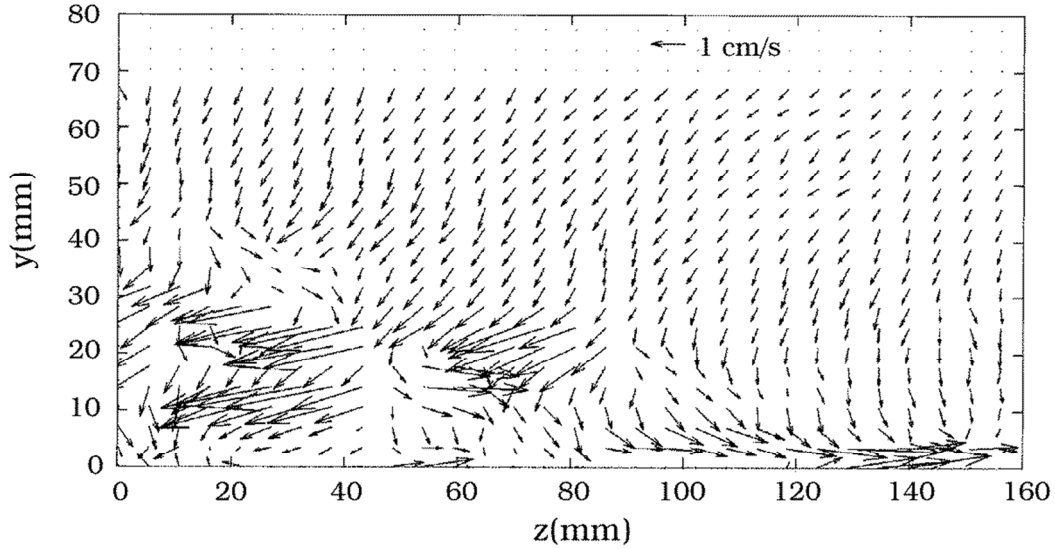

Figure 7: Secondary flow structures close-up of corner section. Test 1.

Mechanism of edge scour

Figure 8 shows the cross flow bed profiles measured at ten sections corresponding to the equilibrium stage of Test 1. The results show considerable scatter and is due to the ripples. Further to this, the ripples extend over the entire sediment bed. Figure 9 displays the "space-averaged" cross-flow bed profile, averaged over the 10 profiles given in Figure 8. Figure 9 also includes the "time-averaged" profile, obtained at the last section (x = 900 mm). As expected, the mean profile obtained by space averaging and that obtained by time averaging practically collapse on a single curve.

Despite the scatter Figure 8 and 9 show following pattern:

1. Scour occurs at the edge of the stone layer (Area B)
2. Deposition occurs inside the toe of the stone layer (Area A)
3. A slight deposition of sediment outside area B (Area C)

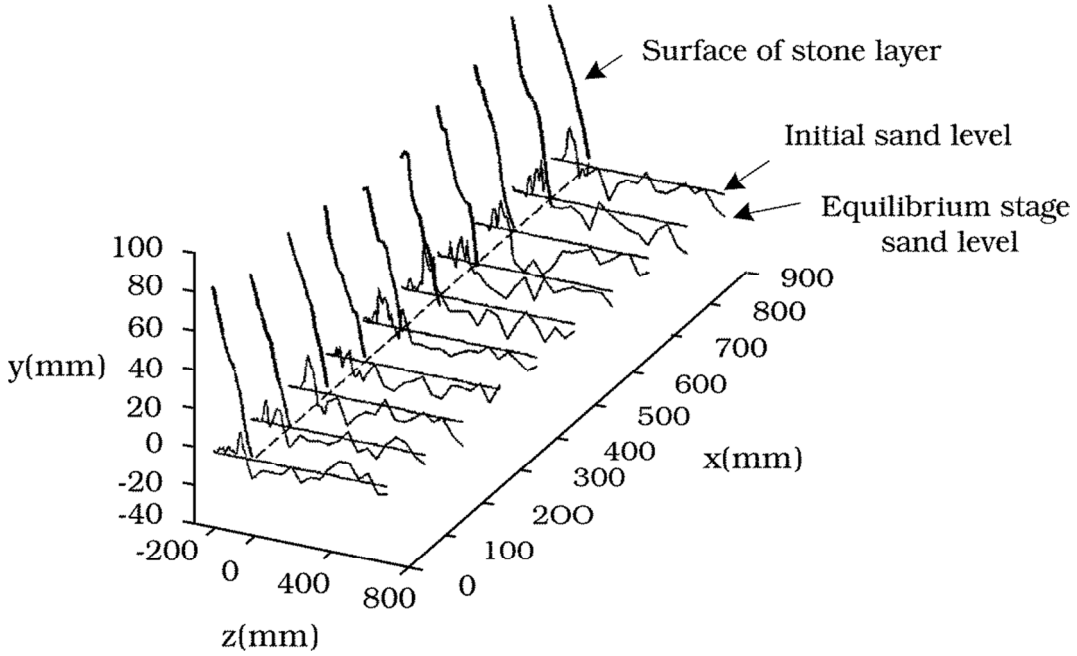

Figure 8: Bed profiles measured at 10 sections across the longitudinal direction. The length of the working section was 1 m. Live-bed ($\theta > \theta_{cr}$). Test 1. Vertical scale is grossly exaggerated.

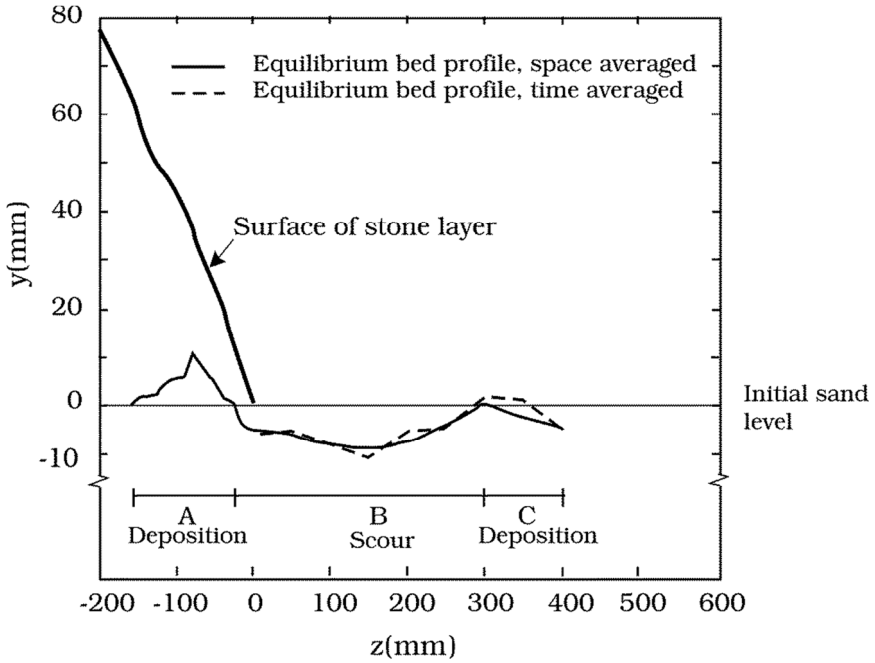

Figure 9: Mean bed profile, space- and time averaged in cross-flow direction. Sketch of scour deposition pattern. Live-bed ($\theta > \theta_{cr}$). Test 1. Vertical scale is grossly exaggerated.

Figures 6 - 9 suggest the governing mechanism of the edge scour as follows. The scour is caused by following two effects: (1) turbulence in the primary flow near the junction between the stone layer and the sand bed; and (2) the secondary flow described in the previous paragraph. Sediment is stirred up by the turbulence and brought up into suspension, and the secondary flow carries the sediment away from the junction between the bed and the stones, resulting in the edge scour.

With this, stones at the edge of the cover stones are "undermined", and as a result slump down into the scour hole.

There are two kinds of turbulence. One source of turbulence in the primary flow mentioned above is that generated in the fully developed turbulent boundary layer over the sand bed and the stone layer. The second

source of turbulence, on the other hand, is the turbulence generated locally around individual stones at the toe, in the form of horseshoe-vortex and lee-wake flow.

As the scour around the stones continues and the process removes sand beneath the stones, stability is lost and therefore the stones slump into the scour hole. In some cases the latter process was accompanied by sinking of the stones caused by shear failure of the sand beneath the stones. Here the sand loses its bearing capacity and the stones sink into the sediment bed.

The displacement of the stones at the edge causes the upper layers of stones to move as well. The stones located at the surface therefore move towards the edge. As a result of this the surface of the sloping stone layer stretches and settles. The observed settlement of the stone layer surface is O(0.3 - 0.5 D_s).

From the video recordings the detailed mechanism of the stone displacement at the toe was observed. The scour holes around the toe stones are caused by contraction of the streamlines at the side edge of the stone and the local enhancement in the turbulence intensity, caused by the horseshoe vortex and the vortex shedding. The formation of the horseshoe vortex and the vortex shedding was revealed by sediment which acted as flow tracers.

As seen clearly from Figures 8 and 9 that sand is infiltrated into the cover stone layer and as a results a substantial amount of deposition takes place inside the stone layer. This is, again, caused by the same mechanism as that causing scour, i.e. the sand stirred up by the turbulence and brought into suspension is carried into the stone layer by the secondary current and deposited there.

V CONCLUSION

Edge scour in a steady current propagating in-line with a stone layer is caused by the combined action of two effects; (1) Primary flow and (2) Secondary flow. The primary flow stirs up the sediment and puts into suspension, and the secondary flow carries it away from the junction between the stone layer and the sand bed, resulting in a scour hole forming adjacent to the toe of the stone layer, Area B in Figure 9.

As a result of this mechanism the sediment is deposited in two locations, Area A and Area C in Figure 9.

VI ACKNOWLEGMENTS

This study was partially funded by (1) Danish GTS-university-cooperation project “Future Marine Structures”; (2) the Danish Council for Strategic Research (DSF)/Energy and Environment Program "Seabed Wind Farm Interaction"; (3) EU FP7-project, MERMAID 28870; and (4) Statkraft thorugh: Statkraft Ocean Energy Research Program (SOERP)(Norway).

VII REFERENCES

Fredsøe, J., Sumer, B. M, Bundgaard, K. (2001). “Scour at a riprap revetment in currents.” Proceedings of 2nd IAHR Symposium on River, Coastal and Estuarine Morphodynamics. 2001, pp. 245-254.

Müller, A., Studerus, X. “Secondary flow in an open channel.” *Proceedings of the 18th IAHR Congress, Cagliari*, **3**: 19-24.

Nezu, I., Nakagawa, H., (1993) “Turbulence in open-channel flows.” A. A. Balkema, Rotterdam.

Hansen, N. E. O., Gislason, K. (2005) ”Movable scour protection on highly erodible sea bottom.” LICengineering A/S, Ehlersvej 24, DK-2900 Hellerup, Denmark.

Raaijmakers, T. C., Oeveren, M. C., Rudolph, D., Leenders, V., Sinjou, W. C. P., (2010) “Field performance of scour protection around offshore monopoles.” Proceedings of the Fifth International Conference on Scour and Erosion, ICSE 2010, pp 428-439.

Sumer, B. M, Fredsøe, J., (2002) ”The Mechanics of Scour in the Marine Environment.” World Scientific, New Jersey, Singapore, London, Hong Kong.

van Rijn, L. C. (2011) “Principles of fluid flow and surface waves in rivers, estuaries, seas and oceans.” Aqua Publication.

Whitehouse R. J. S. (1998) *“Scour at marine structures: A manual for practical applications.”* Thomas Telford, London.

Whitehouse, R. J. S., Harris, J. M., Rees, J. (2011) "The nature of scour development and scour protection at offshore windfarm foundations." *Marine Pollution Bulletin* **62** : 73-88.